Coupled biophysical modeling to understand the spread of a deadly coral disease in Florida

Thomas Dobbelaere [1,*], **Erinn Muller** [2], **Lewis Gramer** [3,4], **Dan Holstein** [5] and **Emmanuel Hanert** [1,6]

[1] Earth and Life Institute (ELI), UCLouvain, Louvain-la-Neuve, Belgium
[2] Coral Health and Disease Program, Mote Marine Laboratory, Sarasota, FL, USA
[3] Cooperative Institute for Marine and Atmospheric Studies (CIMAS), University of Miami, Miami, FL, USA
[4] Atlantic Oceanographic and Meteorological Laboratory (AOML), NOAA, Miami, FL, USA
[5] Department of Oceanography and Coastal Sciences, College of the Coast and Environment, Louisiana State University, Baton Rouge, LA, USA
[6] Institute of Mechanics, material and Civil Engineering (IMMC), UCLouvain, Louvain-la-Neuve, Belgium

Correspondence*:
Earth and Life Institute (ELI), UCLouvain, Croix du Sud 2 box L7.05.16, B-1348 Louvain-la-Neuve, Belgium
thomas.dobbelaere@uclouvain.be

ABSTRACT

For about six years, the Florida Reef Tract (FRT) has been experiencing an outbreak of the Stony Coral Tissue Loss Disease (SCTLD). First reported off the coast of Miami-Dade County in 2014, the SCTLD has since spread throughout the entire FRT with the exception of the Dry Tortugas. However, the causative agent for this outbreak is currently unknown. Here we show how a high-resolution bio-physical model coupled with a modified patch Susceptible-Infectious-Removed (SIR) epidemic model can inform on the potential characteristics of the causative agent of the disease and its vector. In this study, the agent is assumed to be transported within composite material (such as coral mucus, dying tissues and/or resuspended sediments) driven by currents and potentially persisting in the water column for extended periods of time. In this framework, our simulations suggest that the SCTLD is likely to be propagated within neutrally buoyant material driven by mean barotropic currents. Calibration of our model parameters with field data shows that corals are then infected within a mean transmission time of 6.45 days, with a basic reproduction number slightly above 1. Furthermore, the propagation speed of the disease through the FRT is shown to occur for a well defined range of values of an infection threshold, defined as the fraction of infectious corals that causes an exponential growth of the disease in the colony. Our results present a new connectivity-based approach to understand the spread of the SCTLD through the FRT. Such a method can provide a valuable complement to field observations and lab experiments to support the management of the epidemic as well as the identification of its causative agent.

Keywords: stony-coral-tissue-loss disease, biophysical modeling, Florida reef tract, spatial epidemiology, connectivity

1 INTRODUCTION

23 Coral diseases are a major threat to coral reef ecosystems and have led to significant declines in coral
24 cover especially within the Caribbean region (Richardson et al., 1998; Sutherland et al., 2004; Aronson and
25 Precht, 2001; Harvell et al., 2007; Miller et al., 2009; Brandt and McManus, 2009). Indeed, the Florida
26 Reef Tract (FRT), which was dominated by *Acropora palmata* and *Acropora cervicornis*, and often had
27 30% coral cover until the 1970s/80s (Dustan and Halas, 1987; Porter and Meier, 1992), is now dominated
28 by bare substrate, octocorals, and macroalgae with only approximately 5% stony coral cover remaining
29 (Ruzicka et al., 2013). The loss of the branching Acroporid species was attributed primarily to a disease
30 outbreak, termed white band disease (Aronson and Precht, 2001), but several other threats such as habitat
31 reduction, eutrophication, overfishing, hurricanes, and bleaching likely all contributed to these species
32 decline (Team, 2005). Subsequent losses of coral cover within the region were often linked to additional
33 disease incidences and repeated regional coral bleaching events as a result of global climate change (Kuta
34 and Richardson, 1996; Richardson et al., 1998; Sutherland et al., 2004; Gardner et al., 2003; Aronson and
35 Precht, 2006; Kuffner et al., 2015; Manzello, 2015). A novel coral disease outbreak, termed Stony Coral
36 Tissue Loss Disease (SCTLD), is now threatening the last vestiges of coral throughout the Florida Reef
37 Tract (FRT).

38 SCTLD was first documented off the coast of Miami-Dade County in the summer of 2014 by Precht et al.
39 (2016) and has since spread throughout the entire FRT with the exception of the Dry Tortugas. To date,
40 SCTLD has been observed affecting over 20 different stony corals species. A case definition of SCTLD has
41 been compiled to describe the visual appearance and ecology of SCTLD (NOAA, 2018). Briefly, the gross
42 morphology of SCTLD is described as focal or multifocal, with locally extensive to diffuse areas of acute
43 to subacute tissue loss distributed basally, peripherally, or both. In some cases, tissues bordering areas of
44 chronic tissue loss show indistinct bands (1–5 cm) of pallor, progressing to normal pigmentation away from
45 the denuded skeleton. There is also a range in coral susceptibility to SCTLD, with species categorized as
46 highly susceptible (e.g., Dendrogyra cylindrus, Dichocoenia stokesii, Meandrina meandrites), moderately
47 susceptible (e.g., Orbicella spp., Montastraea cavernosa, Siderastrea siderea, Stephanocoenia intersepta), or
48 tolerant (e.g., Porites spp., Acropora spp.). Unfortunately, SCTLD has not remained isolated in the FRT
49 and has now been recorded in Mexico (Alvarez-Filip et al., 2019), the US Virgin Islands (Blondeau et al.,
50 2020) and several other locations around the Caribbean (Kramer et al., 2019). The continued persistence of
51 the outbreak, the high number of species affected, and the large geographical range of reports consistent
52 with the case definition suggests that SCTLD is the largest coral disease outbreak on record

53 Large-scale spatial epidemiologic analyses showed that the reefs in Florida with SCTLD are clustered,
54 supporting a contagious mode of transmission (Muller et al., 2020). Similarly, aquaria-based experiments
55 indicate SCTLD can be transmitted through direct contact or indirectly through the water column (Aeby
56 et al., 2019) suggesting water can be a SCTLD vector, at least within a controlled setting. The initial
57 exponential increase in spread among reefs from the disease epicenter (Precht et al., 2016) and the persistent
58 subsequent linear rate of spread of SCTLD (Muller et al., 2020), north along South Florida reefs and south
59 into the Florida Keys, indicates that water currents may play a role in disease transmission. Furthermore,
60 the rate of spread, estimated at 100 m per day, suggests surface currents are likely too fast to have spread
61 SCTLD within the region. These results imply that the bottom boundary layer, which is significantly
62 slower than surface currents, may be the vertical location in which transmission occurs (Aeby et al.,
63 2019). However, to date, there have been no attempt to link local hydrodynamic modeling efforts with the
64 spatio-temporal dynamics of SCTLD in Florida.

Estimating the transport of the disease causative agent from reef to reef by currents cannot be performed empirically. However, experimentally-calibrated numerical models that simulate currents can provide a realistic picture of the dispersal of disease agents. Nonetheless, accurately modeling water circulation at the spatial scales that affect this dispersal remains a key challenge, as small-scale flow features such as recirculation eddies around reefs and islands strongly impact exchanges between reefs (Wolanski, 1994; Burgess et al., 2007; Figueiredo et al., 2013). In this context, models that can explicitly simulate flow features down to the reef scale are needed. This represents a spatial resolution of the order of 100-1,000 m in dense reef systems. As of today, most regional ocean models using traditional numerical methods cannot achieve such resolution because of the computational resources it requires. To our knowledge, the best resolution currently available among these models in the FRT is ~ 900 m with the FKEYS-HYCOM model that has been developed for the Florida Keys region (Kourafalou and Kang, 2012; Sponaugle et al., 2012; Vaz et al., 2016). Unstructured-mesh ocean models offer a potential solution to this resolution issue by locally increasing the model resolution close to reefs and islands (Lambrechts et al., 2008; Thomas et al., 2014, 2015), in order to focus the computational resources where they are most needed. High resolution bio-physical dispersal models can be used to build the potential connectivity between reefs and therefore approximate exchanges between colonies in the complex topography of the coral reef systems (Frys et al., 2020).

Marine diseases differ significantly from better studied terrestrial diseases, namely due to the potential for long environmental residence times, during which pathogens may survive and disperse through the water (Harvell et al., 2007; Sokolow et al., 2009). Several recent studies have attempted to adapt traditional epidemic models (Susceptible-Infectious-Recovered, or SIR models) to coral reef systems (Sokolow et al., 2009; Bidegain et al., 2016a,b). Novel approaches have included developing pathogen pools (Bidegain et al., 2016a,b), and to model at the metapopulation scale, rather than at the scale of coral holobionts (Sokolow et al., 2009). Both of these approaches are attempting to address the same issue: infection occurs between patches of entirely sessile animals, through the dispersal of pathogen(s). Thus, there are internal within-patch disease dynamics and metapopulation-scale between-patch dynamics occurring simultaneously. The epidemic model developed in this study utilizes the same basic architecture of previous coral reef SIR models, but rather than assume pathogen pools (e.g. Bidegain et al. (2016a,b)) or ignore internal patch dynamics (e.g. Sokolow et al. (2009)), we have modeled both within-patch disease dynamics and the dispersal of pathogens explicitly using potential connectivity networks.

The objective of this study is to deduce the probable propagation mechanism of the SCTLD throughout the FRT by developing an experimentally-calibrated epidemio-hydrodynamic model. With a resolution of about 100 m, this model can capture potential exchanges of disease-carrying material, further denominated as "infectious" in our modeling framework, between reefs that would be ignored by coarser models. By reproducing the observed spread of disease between 1st May 2018 and 1st April 2019, we provide insight on the characteristics of the disease agent and its vector. Ultimately, our model, coupled with lab and field works, would support the management of the epidemic and the identification of its causative agent.

2 METHODS

2.1 Modeling reef connectivity

In this study, we focus on the exchanges of infectious material between coral reefs driven by ocean currents, which therefore have to be accurately simulated. An ocean model should provide a realistic large-scale circulation while also resolving small-scale flow features down to the scale of individual reefs.
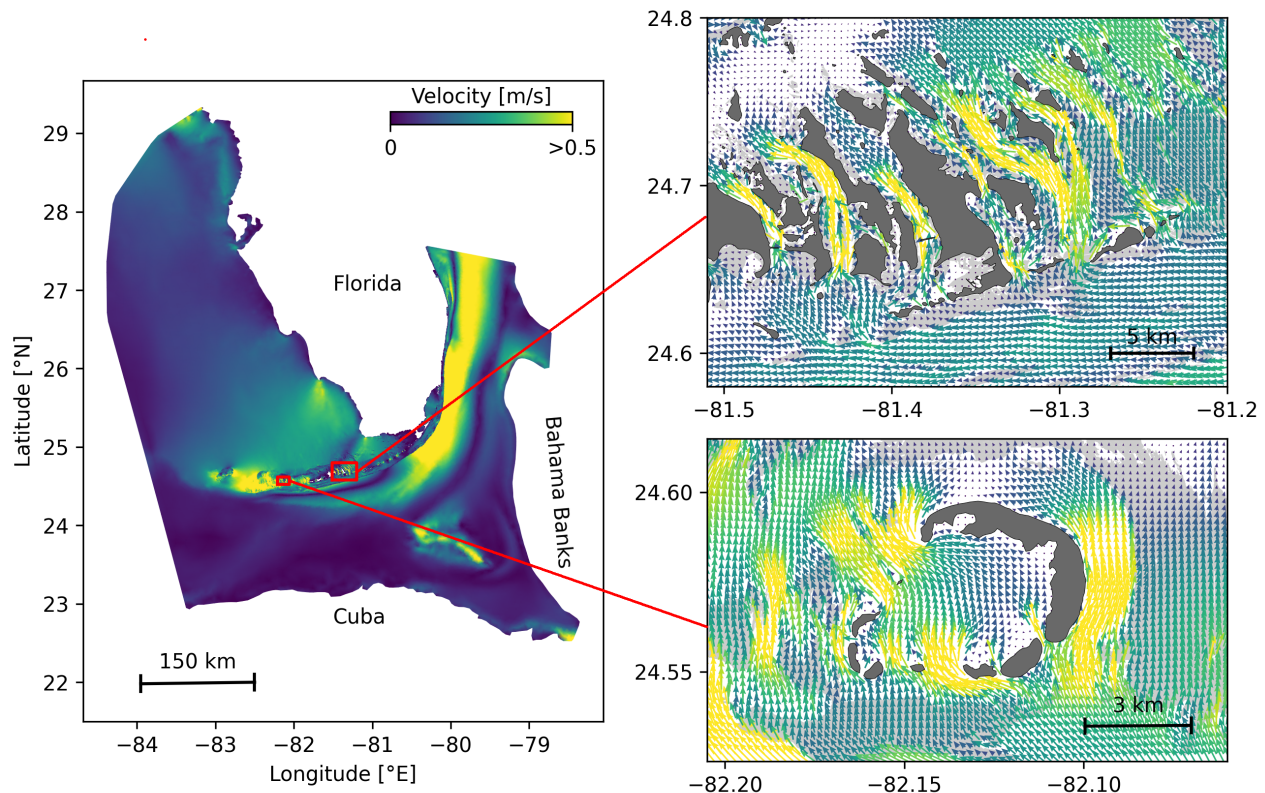
Figure 1. Model computational domain and close-up views of the mesh with snapshots of the currents on May, 25 2018 at 00:00, for the Marquesas Keys (bottom) and the Lower Keys (top). This illustrates the benefits of unstructured meshes to represent the fine-scale details of the topography and hence simulate currents down to the scale of individual reefs (shown in light grey) and islands (shown in darker grey).

106 In this context, we use the unstructured-mesh depth-integrated coastal ocean model SLIM [1] to simulate
107 ocean currents over an area that includes the FRT but also the Florida Strait and part of the Gulf of Mexico
108 (Fig. 1). By using an unstructured mesh, we can increase the model resolution only over the FRT and hence
109 concentrate computational resources where they are most needed. SLIM has already been successfully
110 applied in complex coastal systems such as the Great Barrier Reef (Lambrechts et al., 2008; Thomas
111 et al., 2014) and is well suited to shallow-water flows. Details of the model formulation and validation are
112 provided in Frys et al. (2020).

113 The mesh resolution depends only on the distance to the coast, but we distinguish between the coastlines
114 along the FRT where we impose a maximum resolution of 100 m and the other coastlines along which the
115 finest resolution is 2500 m. The mesh has been generated with the open-source mesh generator GMSH
116 (Geuzaine and Remacle, 2009) and has about 7×10^5 elements. The coarsest elements, far away from the
117 FRT, have a characteristic length size of about 10 km. An illustration of ocean currents simulated on that
118 mesh are shown in Fig. 1. It shows how a 100-m spatial resolution allows us to simulate fine-scale details
119 of the flow, such as recirculation eddies and currents within the dense reef system in the Lower Keys that
120 consist of many individual reefs with narrow passages in between.

121 The simulated currents can then be used to model dispersal of infectious material throughout the FRT.
122 In this study, 3 types of potential vector carrying the disease causative agent were considered: positively

---

123 buoyant (e.g. mucus and surfactant), neutrally buoyant (e.g. fines, pelagic organisms) and negatively
124 buoyant (e.g. sediments, composites, demersal organisms). As SLIM is a depth-averaged model, the
125 mean currents it generates are well suited to model the dispersal of neutrally buoyant material remaining
126 within the water column. However, these currents must be modified to correctly represent the dynamics of
127 material evolving in the surface and bottom boundary layers. Therefore, surface current response to winds
128 is estimated by adding 1.5% of the wind speed to SLIM currents with a stress-layer veering angle of $45°$ to
129 the right for positively buoyant particles. Such parameterization is shown to be an accurate approximation
130 of wave-induced Stokes drift and quasi-Eulerian surface currents by Ardhuin et al. (2009). For negatively
131 buoyant material, on the other hand, bottom currents are obtained by taking 60% of SLIM currents velocity
132 with a veering angle of $15°$ to the left. This is an approximation based on observations of bottom currents
133 and whole water column current profiles in the shallow waters (<15 m) of Hawk Channel in the middle
134 Florida Keys by Smith (2009), as well as observations obtained during the Atlantic Ocean Acidification
135 Testbed project (Gramer, pers. comm.). It is also consistent with the theory of current veering in the bottom
136 Ekman layer, albeit that was previously observed in deeper (30-90 m) coastal waters, e.g., by Perlin et al.
137 (2007) and Kundu (1976).

138   Using these three velocity fields, virtual particles are then released on all the reefs composing the FRT to
139 model the dispersal of infected material carrying the disease causative agent. The locations of the reefs of
140 Florida are extracted from the "coral reefs and hardbottom" layer of the Unified Florida Reef Tract Map
141 (FWC-FWRI, 2017). The polygons of this reef map are then further divided into 500 m × 500 m squares
142 in order to track the propagation of the disease with a finer geographical resolution, generating a total of
143 16,823 polygons. At the beginning of each simulated month and for each type of current, a total of about
144 1.5×10^6 particles are released over all the reef polygons. These particles have a state composed of their
145 polygon of origin as well as their mass, that they loose at a constant rate γ as they are moved by surface,
146 mean or bottom currents. In this study, the value of γ is chosen so that particles have a half life of 30 days.
147 When the particles are brought over a reef polygon by currents, the amount of infected mass that lands on
148 the polygon is recorded in monthly potential connectivity matrices, whose entries are denoted C_{ij}. The
149 matrix rows correspond to the source reefs and the columns correspond to the destination reefs. Hence C_{ij}
150 represents the mass of diseased material originating from sub-reef i that has settled on sub-reef j. This
151 matrix is then normalized by dividing each of its rows i by the total mass of particles released on polygon i
152 in order to obtain the normalized potential connectivity matrix $\tilde{C}$, whose entry $\tilde{C}_{ij}$ gives the probability
153 that disease agents produced on sub-reef i settle on sub-reef j. Connectivity matrices are computed for
154 each type of current and for each month of the simulated period.

155   These connectivity matrices can be more easily handled by interpreting them as large graphs whose
156 vertices are sub-reefs and whose edges represent connectivity pathways. They can then be analyzed using
157 graph theory tools. In this study, four potential connectivity measures are used to interpret the monthly
158 computed graphs. These indicators are described in Table 1. The first indicator is the weighted connectivity
159 length (WCL), that gives the average dispersal distance from origin to destination for material produced on
160 a given reef. The weighted connectivity of reef polygon i writes:

$$\text{WCL}_i = \frac{\sum_j \tilde{C}_{ij} L_{ij}}{\sum_j \tilde{C}_{ij}} \tag{1}$$

161 where L_{ij} is the distance between origin reef i and destination reef j. Another measure of the spreading
162 potential of reef j is its out-degree, *i.e.* the product of the number of connections originating from reef
163 j by the quantity of infectious material it sends to the network. This indicator is obtained by computing

Indicators	Description	What it shows
Weighted connectivity length (WCL)	Average dispersal distance from origin to destination reef for all disease agents released over a reef	Average distance at which a reef can send disease agents
Out-degree	Number of out-going connections originating from a given reef multiplied by the total mass exchanged	Potential for a reef to spread the disease
Fraction exchanged	Fraction of infectious material produced on a given reef that settles on other reefs	Success rate of potential disease spread
Self recruitment	Fraction of infectious material settling on a given reef that has been released on the same reef	Potential for disease to settle on reef

Table 1. Indicators used to analyze the modeled exchanges of infected material for each considered type of currents and for each simulated month

164 the number of non-zero entries of row i in the potential connectivity matrix C and multiplying it with
165 $\sum_j C_{ij}$. The information given by the out-degree is complemented by the fraction of infectious material
166 produced on reef i that successfully settles on a reef, called the fraction exchanged of reef i. This indicator
167 is given by $\sum_j \tilde{C}_{ij}$. Finally, the isolation of reef i in the network is given by its self recruitment, *i.e.* the
168 fraction of infectious material settling on reef i that originates from reef i, computed by $C_{ii}/\sum_j C_{ji}$. A
169 large self-recruitment value indicates that little infectious material produced elsewhere settles on the reef
170 and thus that it is isolated from the rest of the network.

171 **2.2 Epidemiological modeling**

172 2.2.1 Model equations

173   The spread of the SCTLD throughout the FRT is simulated using a connectivity-based Kermack and
174 McKendrick (1927) SIR model. SIR models are among the most standard epidemiological models. They
175 divide individuals into three compartments: susceptible (S), infectious (I) and removed (R). When affected
176 by the disease, susceptible individuals become infectious and infect other susceptible individuals until
177 they are removed from the system, either through recovery or death. Such models usually rely on the
178 hypothesis of an homogeneous, well-mixed population. To account for the spatial heterogeneity of the
179 FRT, the basic SIR formulation is here modified by considering the fractions of susceptible (S_j), infectious
180 (I_j) and removed (R_j) corals of each sub-reef j. In this epidemiological model, individual reefs interact
181 through the exchange of infectious material as represented by the different connectivity matrices. For each
182 sub-reef j and at any time, the following relations hold: $0 \leq S_j, I_j, R_j \leq 1$ and $S_j + I_j + R_j = 1$. The
183 evolution of these fractions through time is governed by the following equations:

$$\frac{dS_j}{dt} = -\beta \sum_i \frac{A_i}{A_j} I_i \tilde{C}_{ij} S_j - \beta'(I_j) S_j I_j$$

$$\frac{dI_j}{dt} = \beta \sum_i \frac{A_i}{A_j} I_i \tilde{C}_{ij} S_j + \beta'(I_j) S_j I_j - \sigma I_j \qquad (2)$$

$$\frac{dR_j}{dt} = \sigma I_j$$

184 where $\tilde{C}_{ij}$ is the entry corresponding to reef pair (i, j) of the normalized potential connectivity matrix [-],
185 A_i is the area of reef polygon i [km^2], σ is the mortality rate [day^{-1}], and β and $\beta'(I_j)$ are the inter- and
186 intra-reef disease transmission rates [day^{-1}], respectively. In this model, infectious corals of sub-reef i can
187 infect corals of sub-reef j if there is non-zero probability of infectious material exchange from sub-reef i to
188 sub-reef j, given by $\tilde{C}_{ij}$. Moreover, to account for coral resistance to the disease, the intra-reef transmission
189 function $\beta'(I_j)$ has the shape of a smooth step function of the fraction of infectious corals I_j and writes:

$$\beta'(I_j) = \frac{\beta'_0}{2}(1 + \tanh[(I_j - I_0)/\tau]), \tag{3}$$

190 where I_0 is a threshold on the infection population above which intra-reef transmission becomes significant,
191 and τ is a measure of the interval over which the transition from low to high transmission occurs. As long
192 as the fraction of infectious corals on sub-reef j is below I_0, the only infection mechanism taking place
193 is connectivity-driven transmission at rate β. Once the threshold is approached, intra-reef transmission
194 with rate β'_0 is activated. A larger value of threshold I_0 corresponds to a greater resistance of corals to
195 the disease, and therefore a slower spread of the disease within reef j. Coral birth and natural (*i.e.* non
196 SCTLD-related) death rates are not taken into account in this model, which amounts to assume that they
197 balance each other. For this study the same values were used for β and β'_0.

198 ### 2.2.2   Calibration

199   Transmission and removal parameters β'_0 and σ are fitted to disease prevalence observations averaged
200 over all colonies from 6 permanent monitoring sites in the Lower Keys in order to accurately simulate the
201 temporal evolution of S_j, I_j, R_j on each infected reef polygon. Three focal reef sites were established in
202 the lower Florida Keys, one offshore (Acer 17/18), one mid-channel (Wonderland), and one nearshore reef
203 (N. Birthday). Sites were established in May 2018, when all colonies appeared healthy. Within each site,
204 two 10 m $\times$ 10 m quadrats were established. They were generally set up from east to west although N.
205 Birthday was established with one quadrat further north of the other two to better capture coral cover in the
206 site. All coral colonies > 10 cm in size were mapped using self-contained underwater breathing apparatus
207 (SCUBA). Each coral was given an (x, y) coordinate, identified to species, and maximum diameter was
208 noted. After the initial data collection surveys, each site was visited every two to three weeks for rapid
209 assessments to determine whether SCTLD was present. During these site visits, two divers conducted a
210 visual assessment at each of the 6 quadrats. Disease was first observed in early October 2018. Detailed
211 surveys were conducted every two to four weeks until December 2019. During the surveys, each individual
212 coral was visually assessed for signs of SCTLD, including discoloration and tissue loss. Prevalence of
213 diseased, apparently healthy, and dead were assessed for each time period. To relate our model framework
214 to the compiled data, Eqs. 2 are simplified to a single-reef SIR model:

$$\begin{aligned}
\frac{dS}{dt} &= -\beta'_0 SI \\
\frac{dI}{dt} &= \beta'_0 SI - \sigma I \\
\frac{dR}{dt} &= \sigma I
\end{aligned} \tag{4}$$

215 Due to the low values of the entries in the normalized connectivity matrix $\tilde{C}_{ij}$, intra-reef transmission,
216 when activated, is the dominant infection mechanism of Eqs. 2. Consequently, Eqs. 4 give a reasonable
217 approximation of the evolution of the disease on sub-reefs for which $I_j > I_0$. Using this approximation, the

218 ratio β_0'/σ is imposed by matching the modeled fraction of susceptible corals remaining after the disease
219 has vanished (S_∞) with observations. A standard property of a SIR model solution is indeed that

$$S_\infty - \frac{\sigma}{\beta_0'} \log(S_\infty/S_0) = 1 \tag{5}$$

220 where the initial fraction of susceptible corals (S_0) is taken equal to $1 - I_0$ (see for instance Murray (2007)).
221 In the framework of Eqs. 4, the ratio β_0'/σ gives the value of the basic reproduction number R_0, defined as
222 the average number of secondary cases produced by one infected individual introduced into a population of
223 susceptible individuals (Keeling and Rohani, 2007). This number is used in epidemiological models to
224 determine whether an emerging infectious disease can spread in a population ($R_0 > 1$) or not ($R_0 < 1$).
225 The obtained basic reproduction number is then used to express σ in terms of β_0' and calibrate its value
226 in order to reproduce as well as possible the temporal evolution of the colonies-averaged susceptible
227 population shown in Fig. 5.

2.2.3 Initialization

229 In order to solve Eqs. 2, initial conditions are needed, *i.e.* fractions of susceptible, infectious and recovered
230 corals at the beginning of the simulated period. This information is constructed based on 9 different field-
231 collected datasets: (i) Coral Reef Evaluation and Monitoring Project (CREMP; 2014–2017), (ii) CREMP
232 Presence/Absence Data (CREMP P_A; 2016–2017), (iii) Southeast Florida Coral Reef Evaluation and
233 Monitoring Project (SECREMP; 2014–2017), (iv) Florida Reef Resilience Program Disturbance Response
234 Monitoring (FRRP; 2014–2017), (v) Hurricane Irma Rapid Reef Assessment (IRMA; 2017, Viehman et al.
235 (2018)), (vi) the Southeast Florida Action Network citizen science program (SEAFAN; 2014–2017), and
236 (vii) the Southern Coral Disease Margin field effort (2017 and 2018; Neely (2018)), (viii) Mote Marine
237 Laboratory's Field operations data (2018-2019) and (ix) data compiled through Mote's citizen science
238 BleachWatch program (2018). Every dataset provided data on the presence or absence of the SCTLD (or
239 tissue loss consistent with the SCTLD case definition) within each survey. Some also provided detailed
240 disease metrics such as the species affected and the disease prevalence, which was subsequently compiled
241 into presence/absence of SCTLD data by surveyed site. The locations of these observations are shown in Fig.
242 2. Using this information, we first delineate an infected zone by constructing the concave hull of the points
243 where the disease was observed before May 2018. The reefs infected prior to the beginning of our simulated
244 period are then defined as the reefs located inside the constructed zone. The time of observed infection is
245 then spatially interpolated on each reef of the infected zone by kriging with a Gaussian semivariogram
246 using Python `pyKrige` module (Murphy, 2014). Assuming an initial state $(S, I, R) = (1 - I_0, I_0, 0)$
247 when the disease was observed, the fractions of susceptible, infectious and removed corals on each reef of
248 the infected zone on the 1st May 2018 is finally approximated using Eqs. 4. Reefs outside of the infected
249 zone are initialized with an entirely susceptible population.

2.2.4 Computation of front speed

251 Muller et al. (2020) estimated the speed of the spreading STCLD epidemics at around 92 m/day in the
252 southern section of the FRT. In order to assess our simulation results in regard to this value, we developed
253 a methodology to compute the displacement of the disease front during a given time interval within our
254 simulated period. First, the concave hull H_0 of the infected polygons at the beginning of the time interval
255 is delineated. Then the concave hull H_1 of the polygons infected during the time interval is computed
256 while the concave hull H_2 is defined as the union of H_0 and H_1. This methodology is illustrated in Fig. 3.
257 The distance traveled by the disease front is then obtained by computing the maximum distance between
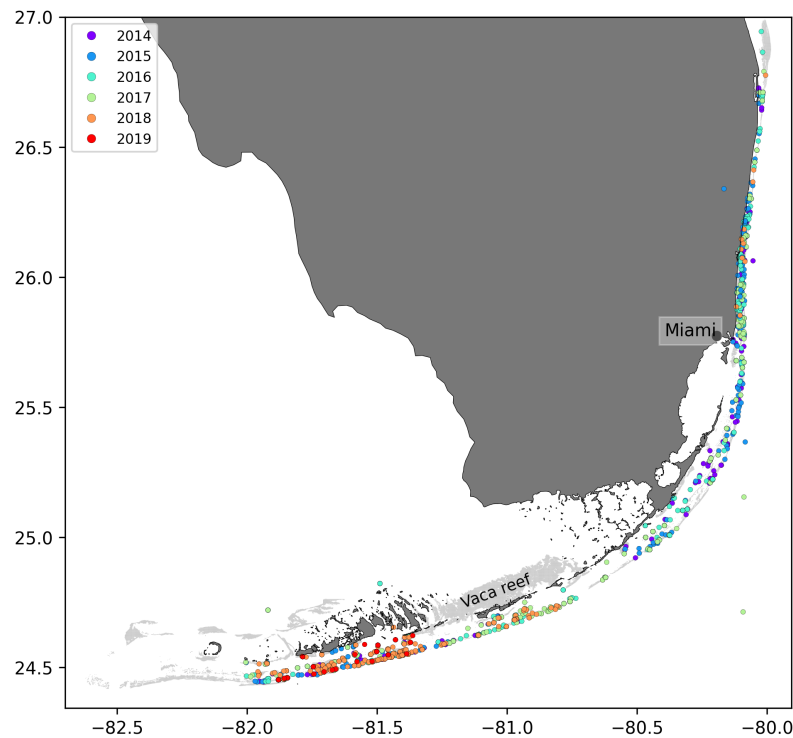
Figure 2. Locations of the disease observations between 2014 and 2019 recorded in the data sets used in this study
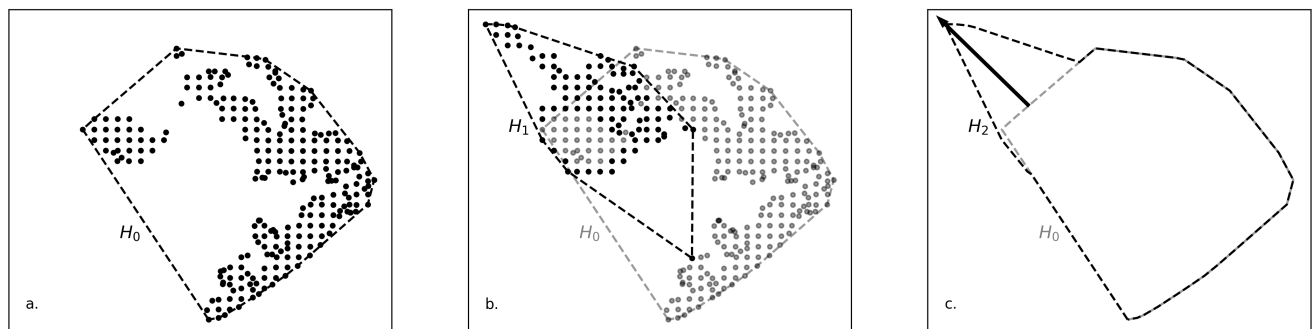

Figure 3. Method used to compute the disease front displacement during a simulated time interval.**a.** Concave hull H_0 of the infected sub-reefs at the beginning of the simulated period. **b.** Concave hull H_1 of the sub-reefs infected during the simulated time interval. **c.** Arrow showing the computed front displacement during simulated time interval between H_0 and H_2, the union of H_0 and H_1.

258   all pairs of points of H_0 and H_2. The epidemics front speed is finally obtained by dividing the resulting
259   distance by the number of days in the simulated time interval.

2.3   Transmission experiments

261   In parallel to this modeling study, laboratory-based transmission experiments of SCTLD were conducted
262   by several independent groups for various end points including transmission dynamics and samples
263   for molecular and histological analysis. Requests for transmission data were sent to members of the
264   'Transmission' sub-group of the Florida Disease Advisory Committee's 'Research' working group as well
265   as any other additional researchers that may have been conducting transmission studies on SCTLD. Data

266 that was requested and subsequently provided included the location, dates, and duration of the experiment,
267 the species used as the diseased colony (donor of disease agents) and apparently healthy colony (exposed to
268 disease agents), the number of successful transmissions as well as the incubation period following a contact
269 with disease agents prior to disease signs. Additional information included the size of the colonies used in
270 the experiment, the percent tissue loss of the diseased (donor) colony at beginning of the experiment, and
271 whether the apparently healthy (exposed) fragment was touching the diseased colony or not.

272 The average probability of successful disease transmission was determined by taking the mean of the
273 number of colonies exposed to the disease in each study divided by the total number of coral colonies
274 exposed to diseased colonies. The 'incubation' period was identified as the average number of days after an
275 apparently healthy coral colony was exposed to a diseased colony before visual disease signs occurred (i.e.,
276 active tissue loss). Only corals that eventually showed disease signs were integrated within the incubation
277 period calculation.

278 Data was provided from 8 different research groups representing 15 institutions and 19 total collaborators
279 providing a total of 109 data points (see table 2 in appendix). After amalgamating the contributed data,
280 the mean probability of transmission of SCTLD to an apparently healthy coral had a likelihood of
281 approximately 44.8 ± 3.6 %. The probability of transmission ranged from 0 to 100% depending on the
282 experiment. Additionally, the time between exposure of an apparently healthy coral to a diseased coral and
283 subsequently showing initial signs of tissue loss (i.e., incubation period) was 9.7 ± 1 days.

3 RESULTS

3.1 Exchanges of infected material

285 Among the three modes of transport, bottom currents exhibited the lowest propagation range as they
286 generate the networks with the smallest weighted connectivity length (Fig. 4). However, infectious material
287 transported by bottom currents has the largest settlement success rate as these currents generate the graphs
288 with the largest fraction exchanged. Therefore, bottom currents tend to transport more infectious material
289 on closer reefs compared to the two other modes of transport. Mean and surface currents, on the other hand
290 showed similar spreading ranges with mean WCL of 20.63 km and 21.39 km respectively. However, the
291 infectious material that surface currents transport have the weakest probability to successfully settle on
292 reefs. Consequently, surface currents and bottom currents produce networks with similar mean out-degree,
293 although surface currents have the potential to transport infectious material on larger distances. Nonetheless,
294 networks have larger median out-degree with bottom currents than with surface currents, which suggests
295 that surface currents have a lower spreading potential than bottom currents. As a result of their large WCL
296 and fraction exchanged, barotropic currents on the other hand exhibit the largest mean out-degree, which
297 indicates that they have the strongest dispersal potential.

298 Self recruitment gives the fraction of infectious material settling on a reef that was produced on the same
299 reef. The greater its values, the more the reef is isolated from the rest of the network. Since infectious
300 material is less likely to settle on isolated reefs, self recruitment informs on the potential for the disease to
301 reach a given reef, whereas all three other indicators inform on the reef spreading potential. Fig. 4 shows
302 that the disease is more likely to settle on the reefs of networks generated by mean currents. This result is
303 consistent with the values of the other connectivity measures, as reefs tend to be more strongly connected
304 with mean currents. On the other hand, reefs are more isolated with bottom currents, as they produce the
305 graphs with lowest WCL and out-degree. Finally, surface currents generate larger self recruitment values
306 than mean currents as they exhibit the lowest fraction exchanged. Therefore, although bottom currents
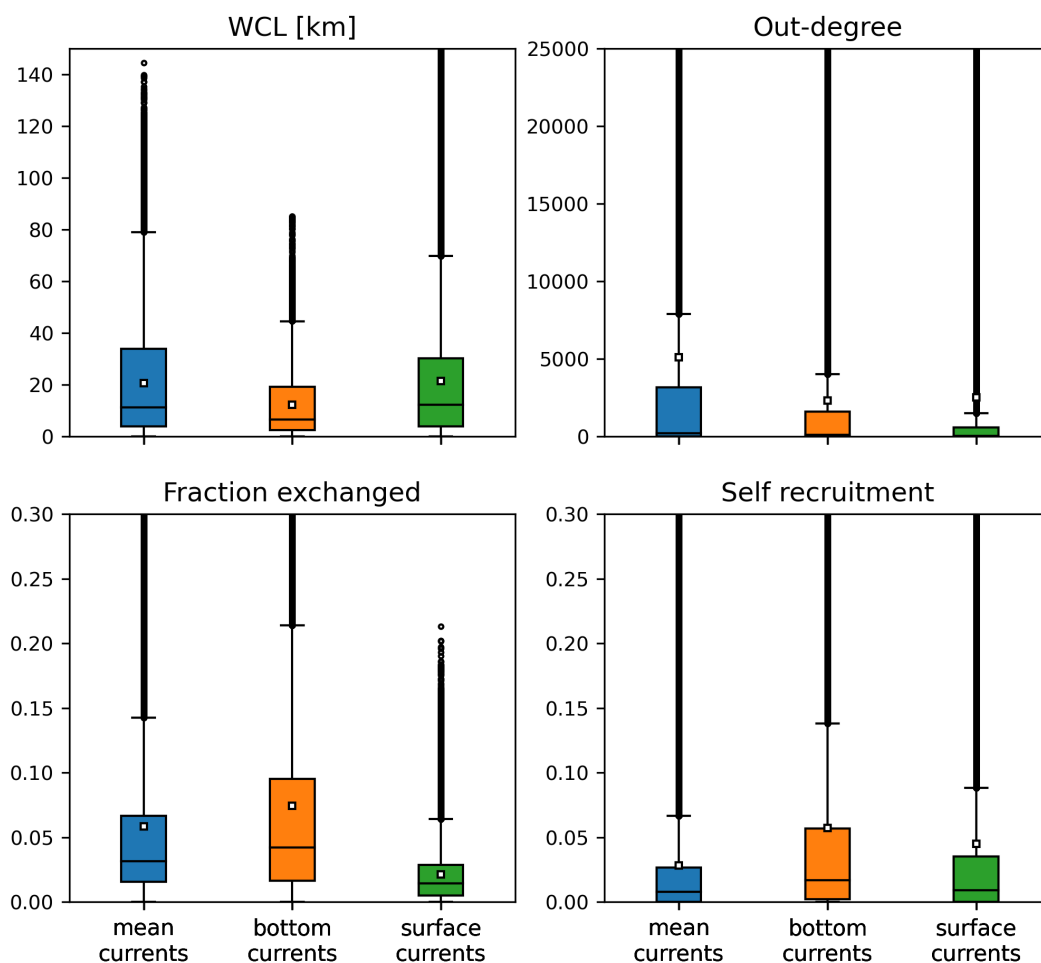
Figure 4. Distribution of the indicators derived from the monthly connectivity matrices computed for each type of current during our simulated period. Mean values are indicated by white squares

exhibit stronger spreading potential than surface currents, reefs are more sensitive to infection with surface currents.

3.2 Epidemiological model results

As aggregated observations show a fraction of susceptible individuals of about 85% at the end of the outbreak, a basic reproduction number $R_0 = \beta_0'/\sigma = 1.0345$ is found with Eq. 5. Using this ratio, best fit to averaged disease prevalence observations is obtained with transmission rate $\beta_0' = \frac{1}{6.45}$ days^{-1} and mortality rate $\sigma = \frac{1}{6.99}$ days^{-1}. Comparison of the evolution of the state described by Eqs 4 results with observations is shown in figure 5. Our model results accurately reproduce the observed fraction of susceptible individuals on colonies through time. However, the modeled fraction of removed individuals overestimates observations by about 5%. These discrepancies might be explained by the presence of "Unknown" values in our data sets as well as the simplifying assumptions of SIR models. Since infection and removal occur at very close rates, the instantaneous fraction of infectious individuals on the reefs remains low through the outbreak, with a maximum value of about 0.4%.

Once the model calibrated, epidemio-hydrodynamic model simulations were performed from 1st May 2018 to 1st April 2019 for each type of currents and different values of the infection threshold I_0. Two
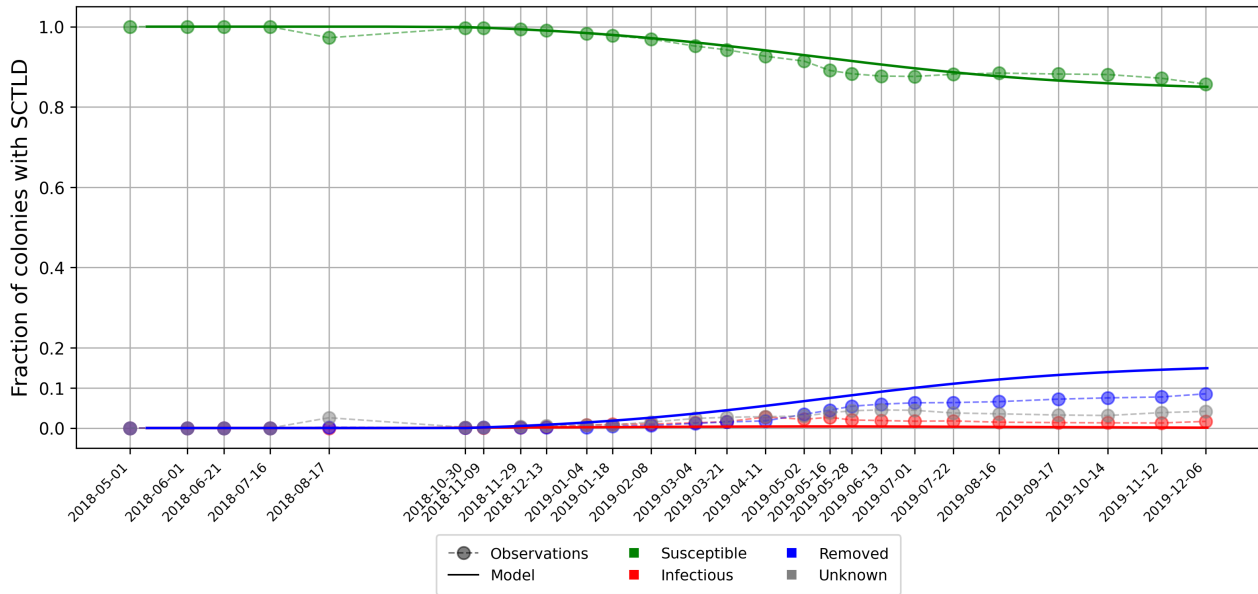
Figure 5. Disease prevalence averaged over all monitored sites over time as modeled by Eqs. 4 using calibrated transmission and removal parameters $\beta'_0 = \frac{1}{6.45}$ days^{-1} and $\sigma = \frac{1}{6.99}$ days^{-1}.

322 metrics were used to assess the accuracy of the model. First, the modeled front speed was compared to the
323 reference rate of 92 m/day derived by Muller et al. (2020). Furthermore, we computed the mean of the
324 distances between each point where SCTLD had been observed during our simulated period (extracted from
325 the 2018-2019 data sets described in section 2.2.3) and the centroid of the closest reef polygon predicted to
326 be infected by our model during the same period (Fig. 6). Bottom currents produced the slowest modeled
327 disease propagation with a maximum front speed of ~ 20 m/day, while simulations performed with surface
328 currents spread the disease at a maximum speed of of about 60 m/day. However, surface currents tend
329 to propagate the disease to the north, rather than westward, along the Florida Keys. This explains why
330 bottom currents predict disease occurance closer to field observations despite exhibiting slower front speed.
331 Finally, mean barotropic currents outperform other types of current predictions regarding both criteria with
332 a front speed of 107 m/day and a mean geographical accuracy of ~ 1.2 km. This suggests that the disease
333 agents of SCTLD may be transported within neutrally buoyant material driven from reef to reef inside the
334 water column by mean currents.

335   Moreover, Fig. 6 shows a strong dependence of the model results to infection threshold I_0, that gives the
336 fraction of infectious individual that colonies can withstand before exponential disease growth is triggered
337 on the reef. Front speeds of both mean and bottom currents reach a plateau for values of infection threshold
338 between $I_0 = 0.05\%$ and $I_0 = 0.1\%$, while the minimal prediction error is reached around $I_0 \approx 0.078\%$
339 with mean currents. For $I_0 > 0.1\%$, intra-reef infection is strongly impeded and populations of infectious
340 individuals on infected reefs are not able to become sufficiently large to infect other colonies on reefs they
341 are connected to. For values of I_0 lower than 0.05% on the other hand, intra-reef infection dominates and
342 coral population on infected reefs is removed too fast to efficiently spread the disease through the network.
343 Since disease propagation throughout the FRT only occurs for fairly small values of I_0 in our model, corals
344 are expected to have low resistance to the causative agent of the SCTLD.

345   The results shown in Fig. 6 were obtained by removing the large reef located North to Vaca key, denoted
346 Vaca reef in Frys et al. (2020), from our reef polygons. Preliminary simulations showed that this reef
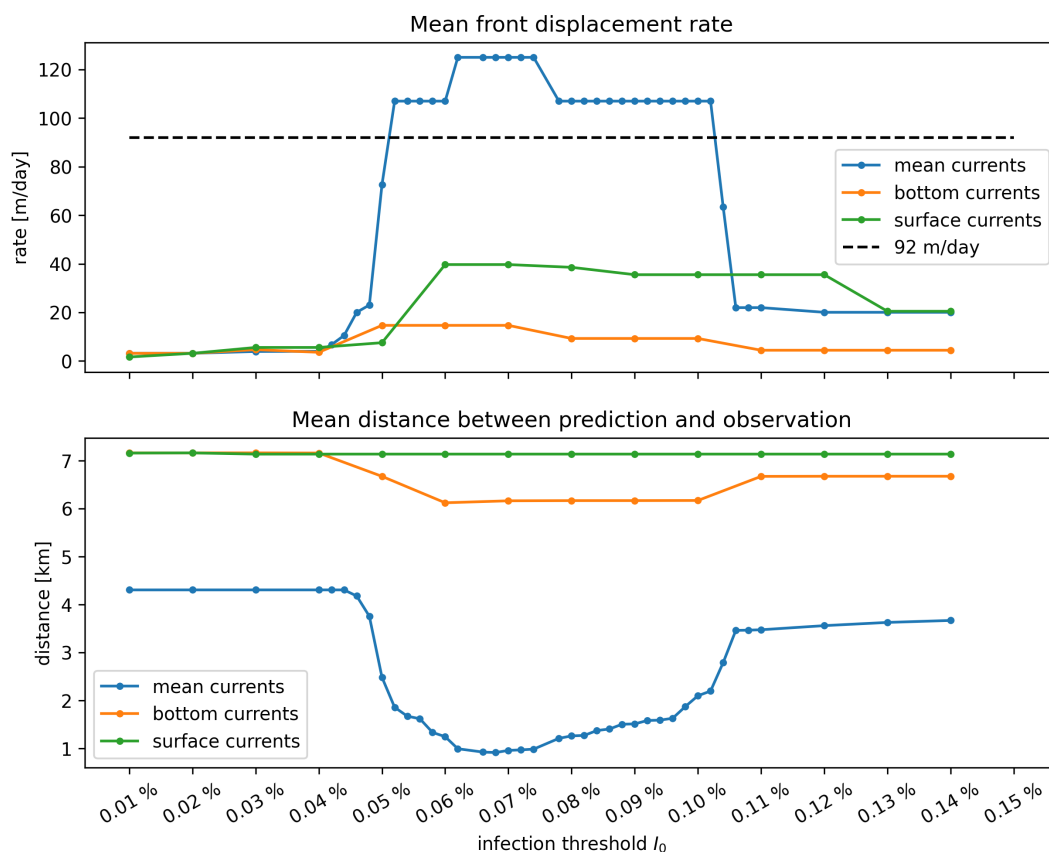
Figure 6. Summary of epidemiological model simulations with calibrated transmission parameters. **Top:** Modeled disease front speed for each type of current with respect to intra-reef infection threshold I_0. **Bottom:** Mean distance between predicted infected reefs and observed disease points. These results show that mean barotropic currents outperform other modes of transport at reproducing the observed spread of the disease. The appearance of a plateau suggests that the modeled spread of the disease occurs for a well-define range of values of I_0.

347 has close to no impact on the modeled spread of the disease to the rest of the FRT, as it sends very little
348 infectious material to southerly and easterly neighboring reefs. Moreover, Vaca reef has a low coral coverage
349 $(0-10\%)$, which strongly impedes disease spread on the reef. However, as coral coverage is not taken into
350 account in our epidemiological model, propagation of the disease on the reef was overestimated. This led
351 to unrealistically strong modeled front speed variations due to the large size of the reef. Consequently, and
352 in the absence of SCTLD observations on Vaca reef, it has been removed from our reef polygons in order
353 to avoid overestimating the front speed.

4 DISCUSSION AND CONCLUSIONS

354 We have developed an epidemio-hydrodynamic model to simulate the spread of the SCTLD through
355 the entire FRT. Calibrating our model with colonies-averaged prevalence observations, we estimated the
356 species-averaged reproduction number R_0 to be slightly larger than one. Our model simulations suggest
357 that only the barotropic currents are able to reproduce the observed spread of the disease. Bottom current
358 do not spread infectious material far enough while surface currents do not allow infectious material to
359 spend enough time over the reefs to strongly affect them. The causative agent of the SCTLD is therefore
360 expected to be transported within neutrally buoyant particles inside the water column. With this mode of

361 transport, the propagation of the disease from reef to reef only occurs for a well-defined range of values
362 of the infection threshold I_0. This threshold is defined as the fraction of all reef colonies that have to be
363 infected to trigger a rapid spread of the disease over the entire reef. Our results suggest that this occurs as
364 soon as $0.05 - 0.1\%$ of colonies are infected. On average, corals are thus expected to have a low resistance
365 to the SCTLD.

366 After calibration, we estimated the species-averaged basic reproduction number β_0'/σ to be equal to
367 1.0835. This value being close to 1, modeled infectious individuals are removed from the system almost
368 as fast as susceptible individuals get infected. This causes the fraction of infectious corals on the reefs to
369 remain pretty low (*i.e.* $\leq 0.4\%$) through time. This suggests that only a small fraction of the colony causes
370 the disease to spread on the reef during the outbreak. The observation-based species-averaged transmission
371 period of 6.45 days used in this model seems to be a reasonable estimation of the disease transmission
372 dynamics as it is of the same order of magnitude as the experimentally-derived mean incubation period
373 of 9.7 days. The difference between the two values can be explained by field measurement uncertainties
374 as well as the inability to perfectly mimic field conditions in laboratory. In this study, the same values
375 were used for inter- and intra-reef rates β and β_0'. This implies that the infectiousness of the causative
376 agent is not reduced during its journey from reef to reef. However, to assess the impact of this assumption,
377 epidemiological model simulations were performed with $\beta = \beta_0'/2$. The resulting disease front speeds
378 did not exceed 20 m/day. This strong decrease can be explained by the interplay between inter- and intra-
379 reef infection. Reducing inter-reef transmission rates decreases the fraction of infectious corals on reefs
380 attained by infectious material, which in turn reduces the amount of infectious material sent to the rest of
381 the network. This suggests that, to reproduce the observed spread, inter- and intra-reef transmission rates
382 must have similar magnitude, *i.e.* that the causative agent is almost not degraded while traveling from reef
383 to reef.

384 The fact that mean barotropic currents outperform the other modes of transport can be explained by
385 considering the trajectories of the particles used to model the transport of the disease causative agent. Due
386 to the impact of winds on positively buoyant material, particles driven by surface currents are likely to be
387 blown away from the reefs. Moreover, even when winds are pushing particles along the reef line, these
388 particles spend less time over the same region than particles driven by mean and bottom currents. Smaller
389 amounts of particle mass will therefore settle on reef polygons, leading to lower entries of the potential
390 connectivity matrix, *i.e.* lower exchange of infectious material between reefs. Hence, despite being able
391 to transport the disease over greater distances, surface currents are less likely to drive the propagation of
392 the disease. Particles driven by bottom currents, on the other hand, remain longer over the same region,
393 producing larger entries of the potential connectivity matrix. Due to these large exchange probabilities
394 between reefs, bottom currents are better at propagating the disease (Fig. 6). Nevertheless, bottom currents
395 being slower, exchanges of infectious material occur on a limited geographical range. Mean barotropic
396 currents, that carry particles on greater distances while allowing for sufficiently large amounts of infected
397 mass to settle on reef polygons, are thus best suited to propagate the disease (Fig. 6).

398 Since mean currents are the only mode of transport that successfully reproduces the observed propagation
399 speed of the disease in our model, the disease causative agent is expected to be transported within neutrally
400 buoyant material inside the water column. Current-driven propagation seems reasonable as water-borne
401 transmission is an important spreading mechanism for multiple coral diseases, including white band disease,
402 white plague disease, white pox disease, white syndrome disease, *Porites* ulcerative white spots diseases,
403 skeletal eroding band disease (Shore and Caldwell, 2019). The causative agent might for instance be
404 transported within fine sediments such as silt, as suggested by Rosales et al. (2020). Such sediments are

405 easily eroded in shallow areas around coral reefs and would therefore be mostly transported inside the water
406 column by mean barotropic currents. This hypothesis might be tested by adapting the deposition rate γ used
407 in our experiments to be consistent with the sedimentation rate of silt. However, such modification of γ
408 would alter the entries of our potential connectivity matrices. Nonetheless, the sensitivity of the connectivity
409 matrices to the value of γ has been briefly assessed by generating new matrices using particles with a
410 half-life of 15 days (γ increased by a factor two). Although these matrices exhibited stronger short-range
411 connectivity, the impact on connectivity indicator values remained limited ($< 10\%$). This suggests that the
412 main results of this study would remain valid for larger deposition rates.

413   Coral resistance to the SCTLD is represented by parameter I_0, defined as the maximum fraction of the
414 colony that can get infected without causing the disease to spread to the rest of the colony. The plateau
415 shown in Fig. 6 highlights the impact of this parameter on the modeled propagation of the disease. On the
416 one hand, when corals are strongly susceptible to the disease, infectious individuals are removed from the
417 system too fast to become sustainable sources of infectious material in the network. On the other hand, if
418 corals are weakly susceptible to the disease, very few corals get infected and the disease barely propagates.
419 Our simulations suggest that this value must be fairly low (around 0.01%) in order to successfully spread
420 the disease throughout the FRT. This seems to imply that susceptible coral species have very weak defense
421 mechanisms against the causative agent of the disease.

422   As with any modeling study, it is important to understand the assumptions on which the model is
423 based. Here, we have used a 2D barotropic ocean model forced by the 3D model HYCOM (Chassignet
424 et al., 2007) in order to indirectly represent baroclinic phenomena. Such model is well suited to simulate
425 the fate of neutrally-buoyant material in shallow regions. However, as depth-averaged currents do not
426 accurately approximate the motion of particles in the bottom and surface layers, they have been modified
427 to simulate the exchanges of negatively and positively buoyant material. Surface current response to wind
428 parameterization is based on the results of Ardhuin et al. (2009), consistent with observations. In this
429 study, measured surface currents are shown to be in the order of $1.0\% - 1.8\%$ of the wind speed, in a
430 direction $10° - 40°$ to the right of the wind. Moreover, the norm and veering angle used to parameterize
431 bottom currents are expected to be reasonably accurate approximations as they are consistent with both
432 Ekman theory and current observations in the Forida Keys (Perlin et al., 2007; Kundu, 1976; Smith, 2009).
433 Although such estimation of surface and bottom currents is disputable, using a 2D model allows for
434 reef-scale resolution throughout the whole FRT. Such high-resolution allows us to explicitly represent
435 recirculation eddies around islands and reefs, that significantly impact the weighted connectivity length as
436 well as the local retention on the reefs.

437   The appearance of an interval of optimal values of threshold I_0 for the propagation of the disease in
438 our results highlights the impact of coral resistance on the spread of SCTLD through the FRT. Therefore,
439 a next step in our modeling approach would be further dividing coral populations of our polygons into
440 highly susceptible (*e.g. Dichocoenia stokesii*, *Meandrina meandrites*), intermediately susceptible (*e.g.*
441 *Orbicella faveolata*, *Montastrea cavernosa*), and weakly susceptible (*e.g. Acropora Palmata*, *Acropora*
442 *cervicornis*) sub-populations. The fractions of susceptible, infectious and removed individuals within these
443 sub-populations would then be modeled with specific transmission (β, β_0') and removal (σ) rates as well as
444 specific infection thresholds I_0. Such approach would however require a fine knowledge of the distribution
445 of the different coral species throughout the FRT. This knowledge about coral coverage could also be used
446 to avoid overestimation of the front propagation, as in the case of Vaca reef.

447   Despite the limitations of its current formulation, we believe that our model brings unprecedented
448 perspectives on the propagation mechanism of the SCTLD through the FRT. Using a reef-scale spatial

449 resolution, we determined the most probable mode of transport for the vector of the disease agent and
450 deduced its species-averaged reproduction number based on prevalence observations. Besides, our model
451 formulation provides a framework to quantify coral resistance to the disease. As our model results are
452 continuous through time, they can exhibit the variability of the propagation of the SCTLD through time
453 and therefore bring additional insight to observation data. This study therefore provides much-needed
454 complementary insight on the identification of the causative agent of the SCTLD and the management of
455 the crisis it generates. Furthermore, our modeling approach could be applied to other affected areas of the
456 Caribbean, where there is still time to perform active management of the disease.

APPENDIX

457 **Transmission data contributors**

Contributors: Transmission Data	Institutions
Erinn Muller*	Mote Marine Laboratory
Katie Eaton*	Mote Marine Laboratory
Jan Landsburg	Florida Fish and Wildlife
Yasu Kiryu	Florida Fish and Wildlife
Esther Peters	George Mason University
Ray Banister	Mote Marine Laboratory/Florida Tech
Valerie Paul	Smithsonian Marine Station
Blake Ushijima*	Smithsonian Marine Station
Nikki Traylor Knowles	University of Miami
Michael Studivan*	University of Miami/NOAA AOML
Joshua Voss	Harbor Branch Oceanographic Institute
Greta Aeby*	Qatar University
Marilyn Brandt*	University of the Virgin Islands
Adrienne Corea	Rice University
Laura Mydlarz	University of Texas - Arlington
Dan Holstein	Louisiana State University
Amy Apprill	Woods Hole Oceanographic Institute
Tyler Smith	University of the Virgin Islands
Sonora Meiling*	University of the Virgin Islands

Table 2. Data contributors to the transmission experiments described in section 2.3, to which the calibrated model parameters were compared. Contributors highlighted with "*" conducted the Data Sharing

CONFLICT OF INTEREST STATEMENT

458 The authors declare that the research was conducted in the absence of any commercial or financial
459 relationships that could be construed as a potential conflict of interest.

AUTHOR CONTRIBUTIONS

FUNDING

ACKNOWLEDGMENTS

REFERENCES

Aeby, G., Ushijima, B., Campbell, J. E., Jones, S., Williams, G., Meyer, J. L., et al. (2019). Pathogenesis of a tissue loss disease affecting multiple species of corals along the Florida Reef Tract. *Frontiers in Marine Science* 6, 678

Alvarez-Filip, L., Estrada-Saldívar, N., Pérez-Cervantes, E., Molina-Hernández, A., and González-Barrios, F. J. (2019). A rapid spread of the stony coral tissue loss disease outbreak in the Mexican Caribbean. *PeerJ* 7, e8069

Ardhuin, F., Marié, L., Rascle, N., Forget, P., and Roland, A. (2009). Observation and estimation of Lagrangian, Stokes, and Eulerian currents induced by wind and waves at the sea surface. *Journal of Physical Oceanography* 39, 2820–2838

Aronson, R. B. and Precht, W. F. (2001). White-band disease and the changing face of Caribbean coral reefs. In *The ecology and etiology of newly emerging marine diseases* (Springer). 25–38

Aronson, R. B. and Precht, W. F. (2006). Conservation, precaution, and Caribbean reefs. *Coral reefs* 25, 441–450

Bidegain, G., Powell, E., Klinck, J., Ben-Horin, T., and Hofmann, E. (2016a). Microparasitic disease dynamics in benthic suspension feeders: infective dose, non-focal hosts, and particle diffusion. *Ecological Modelling* 328, 44–61

Bidegain, G., Powell, E. N., Klinck, J. M., Ben-Horin, T., and Hofmann, E. E. (2016b). Marine infectious disease dynamics and outbreak thresholds: contact transmission, pandemic infection, and the potential role of filter feeders. *Ecosphere* 7, e01286

Blondeau, J., Brandt, M., Donovan, C., Eakin, M., Edwards, K., Edwards, K., et al. (2020). Coral reef condition: A status report for the US Virgin Islands

Brandt, M. E. and McManus, J. W. (2009). Dynamics and impact of the coral disease white plague: insights from a simulation model. *Diseases of aquatic organisms* 87, 117–133

Burgess, S. C., Kingsford, M. J., and Black, K. P. (2007). Influence of tidal eddies and wind on the distribution of presettlement fishes around One Tree Island, Great Barrier Reef. *Marine Ecology Progress Series* 341, 233–242

Chassignet, E. P., Hurlburt, H. E., Smedstad, O. M., Halliwell, G. R., Hogan, P. J., Wallcraft, A. J., et al. (2007). The HYCOM (hybrid coordinate ocean model) data assimilative system. *Journal of Marine Systems* 65, 60–83

Dustan, P. and Halas, J. C. (1987). Changes in the reef-coral community of Carysfort Reef, Key Largo, Florida: 1974 to 1982. *Coral Reefs* 6, 91–106

Figueiredo, J., Baird, A. H., and Connolly, S. R. (2013). Synthesizing larval competence dynamics and reef-scale retention reveals a high potential for self-recruitment in corals. *Ecology* 94, 650–659

Frys, C., Saint-Amand, A., Le Hénaff, M., Figueiredo, J., Kuba, A., Walker, B., et al. (2020). Fine-scale coral connectivity pathways in the Florida Reef Tract: Implications for conservation and restoration. *Frontiers in Marine Science* 7, 312

FWC-FWRI (2017). Unified Reef Map v2. 0. *FWC-FWRI (Florida Fish and Wildlife Conservation Commission-Fish and Wildlife Research Institute)*

Gardner, T. A., Côté, I. M., Gill, J. A., Grant, A., and Watkinson, A. R. (2003). Long-term region-wide declines in Caribbean corals. *science* 301, 958–960

Geuzaine, C. and Remacle, J.-F. (2009). Gmsh: A 3-d finite element mesh generator with built-in pre-and post-processing facilities. *International journal for numerical methods in engineering* 79, 1309–1331

Harvell, D., Jordán-Dahlgren, E., Merkel, S., Rosenberg, E., Raymundo, L., Smith, G., et al. (2007). Coral disease, environmental drivers, and the balance between coral and microbial associates. *Oceanography* 20, 172–195

Keeling, M. and Rohani, P. (2007). Stochastic dynamics. *Modeling Infectious Diseases in Humans and Animals* , 190–230

Kermack, W. O. and McKendrick, A. G. (1927). A contribution to the mathematical theory of epidemics. *Proceedings of the Royal Society of London. Series A, Containing papers of a mathematical and physical character* 115, 700–721

Kourafalou, V. H. and Kang, H. (2012). Florida current meandering and evolution of cyclonic eddies along the Florida Keys Reef Tract: Are they interconnected? *Journal of Geophysical Research: Oceans* 117

[Dataset] Kramer, P., Roth, L., and Lang, J. (2019). Map of stony coral tissue loss disease outbreak in the Caribbean. www.agrra.org. ArcGis Online. (accessed June 12, 2020)

Kuffner, I. B., Lidz, B. H., Hudson, J. H., and Anderson, J. S. (2015). A century of ocean warming on Florida Keys coral reefs: historic in situ observations. *Estuaries and Coasts* 38, 1085–1096

Kundu, P. K. (1976). Ekman veering observed near the ocean bottom. *Journal of Physical Oceanography* 6, 238–242

Kuta, K. and Richardson, L. (1996). Abundance and distribution of black band disease on coral reefs in the northern Florida Keys. *Coral reefs* 15, 219–223

Lambrechts, J., Hanert, E., Deleersnijder, E., Bernard, P.-E., Legat, V., Remacle, J.-F., et al. (2008). A multi-scale model of the hydrodynamics of the whole Great Barrier Reef. *Estuarine, Coastal and Shelf Science* 79, 143–151

Manzello, D. P. (2015). Rapid recent warming of coral reefs in the Florida Keys. *Scientific reports* 5, 16762

Miller, J., Muller, E., Rogers, C., Waara, R., Atkinson, A., Whelan, K., et al. (2009). Coral disease following massive bleaching in 2005 causes 60% decline in coral cover on reefs in the US Virgin Islands. *Coral Reefs* 28, 925

Muller, E. M., Sartor, C., Alcaraz, N. I., and van Woesik, R. (2020). Spatial epidemiology of the Stony-Coral-Tissue-Loss Disease in Florida. *Frontiers in Marine Science* 7, 163

Murphy, B. S. (2014). Pykrige: development of a kriging toolkit for Python. *AGUFM* 2014, H51K–0753

Murray, J. D. (2007). *Mathematical biology: I. An introduction*, vol. 17 (Springer Science & Business Media)

Neely, K. (2018). Surveying the Florida Keys southern coral disease boundary. *Florida DEP. Miami, FL* , 1–15

[Dataset] NOAA (2018). Stony Coral Tissue Loss Disease Case Definition. Available online at: https://nmsfloridakeys.blob.core.windows.net/floridakeys-prod/media/docs/20181002-stony-coral-tissue-loss-disease-case-definition.pdf (accessed June 4, 2020)

Perlin, A., Moum, J., Klymak, J., Levine, M., Boyd, T., and Kosro, P. (2007). Organization of stratification, turbulence, and veering in bottom Ekman layers. *Journal of Geophysical Research: Oceans* 112

Porter, J. W. and Meier, O. W. (1992). Quantification of loss and change in floridian reef coral populations. *American Zoologist* 32, 625–640

Precht, W. F., Gintert, B. E., Robbart, M. L., Fura, R., and Van Woesik, R. (2016). Unprecedented disease-related coral mortality in Southeastern Florida. *Scientific Reports* 6, 1–11

Richardson, L. L., Goldberg, W. M., Kuta, K. G., Aronson, R. B., Smith, G. W., Ritchie, K. B., et al. (1998). Florida's mystery coral-killer identified. *Nature* 392, 557–558

Rosales, S. M., Clark, A. S., Huebner, L. K., Ruzicka, R. R., and Muller, E. (2020). Rhodobacterales and Rhizobiales are associated with stony coral tissue loss disease and its suspected sources of transmission. *Frontiers in Microbiology* 11, 681

Ruzicka, R., Colella, M., Porter, J., Morrison, J., Kidney, J., Brinkhuis, V., et al. (2013). Temporal changes in benthic assemblages on Florida Keys reefs 11 years after the 1997/1998 El Niño. *Marine Ecology Progress Series* 489, 125–141

Shore, A. and Caldwell, J. M. (2019). Modes of coral disease transmission: How do diseases spread between individuals and among populations? *Marine biology* 166, 45

Smith, N. P. (2009). The influence of wind forcing on across-shelf transport in the Florida Keys. *Continental Shelf Research* 29, 362–370

Sokolow, S. H., Foley, P., Foley, J. E., Hastings, A., and Richardson, L. L. (2009). Editor's choice: Disease dynamics in marine metapopulations: modelling infectious diseases on coral reefs. *Journal of Applied Ecology* 46, 621–631

Sponaugle, S., Paris, C., Walter, K., Kourafalou, V., and Alessandro, E. (2012). Observed and modeled larval settlement of a reef fish to the Florida Keys. *Marine Ecology Progress Series* 453, 201–212

Sutherland, K. P., Porter, J. W., and Torres, C. (2004). Disease and immunity in Caribbean and Indo-Pacific zooxanthellate corals. *Marine Ecology Progress Series* 266, 273–302

Team, A. B. R. (2005). Atlantic Acropora status review document. *Report to National Marine Fisheries Service* , 152

Thomas, C. J., Bridge, T. C., Figueiredo, J., Deleersnijder, E., and Hanert, E. (2015). Connectivity between submerged and near-sea-surface coral reefs: Can submerged reef populations act as refuges? *Diversity and Distributions* 21, 1254–1266

Thomas, C. J., Lambrechts, J., Wolanski, E., Traag, V. A., Blondel, V. D., Deleersnijder, E., et al. (2014). Numerical modelling and graph theory tools to study ecological connectivity in the Great Barrier Reef. *Ecological Modelling* 272, 160–174

Vaz, A. C., Paris, C. B., Olascoaga, M. J., Kourafalou, V. H., Kang, H., and Reed, J. K. (2016). The perfect storm: match-mismatch of bio-physical events drives larval reef fish connectivity between Pulley Ridge mesophotic reef and the Florida Keys. *Continental Shelf Research* 125, 136–146

Viehman, S., Gittings, S., Groves, S., Moore, J., Moore, T., and Stein, J. (2018). NCCOS Assessment: Coral Disturbance Response Monitoring (DRM) Along the Florida Reef Tract Following Hurricane Irma From 2017-10-09 to 2017- 10-18 (NCEI Accession 0179071). *NOAA National Centers for Environmental Information* . Silver Spring, MD: National Centers for Coastal Ocean Science. Available online at: https://doi.org/10.25921/sscd-6h41 (accessed June 22, 2020)

Wolanski, E. (1994). *Physical oceanographic processes of the Great Barrier Reef* (CRC Press)